

A Cyclone Database

Project Report – Version 1 - 30th January 2001

Tim Hewson

Accurate prediction of severe weather events is a key Met Office goal. As cyclonic systems are responsible for the vast majority of these events, accurate cyclone prediction is also high priority. Although huge strides have been made in numerical weather prediction (NWP) in recent years, cyclonic systems continue to pose problems for numerical models. Three ‘exceptional’ depressions in the Christmas periods of 1997 and 1999, and another in early December 1999 were all poorly forecast by most of the world’s operational models, indicating that there is plenty of scope for improvement.

The rationale for constructing a cyclone database (previously called the ‘Frontal Wave Database’) is described in detail in Hewson (1998b). The main motivation was the identification and representation of systematic model biases in new formats which, from most practical perspectives, represent a notable improvement on more traditional r.m.s. error-based statistics. Several other possible uses have arisen in the intervening period; these are detailed at the end of this report.

Evidently improved knowledge of cyclone forecast characteristics will be valuable not only to the NWP community, but also to forecasting, in part because operational practice now involves using ‘Field Modification’ software to prepare forecast charts (Carroll, 1997), which can be used to correct for known biases.

The purpose of this report is to describe changes to the project since Hewson (1998b) (section 1.1), to outline the processing stages used to update the database (section 1.2), to describe database structure and list the current set of stored diagnostics (section 2), to pinpoint major problems encountered during the project (section 3), and indeed overall to provide sufficient information for interested parties to comprehend what the database includes and how it can be utilised. Figures from a limited initial analysis of the data are presented in section 4, followed by conclusions (section 5) and proposals describing the possible areas for future work (section 6). A future update of this report will include an expanded section 4.

1. Database Generation

1.1 Changes in Specification

Hewson (1998b) outlined a number of options for database generation, with regard to domain, horizontal resolution, forecast type and computer platforms. We abandoned the plan to work initially on the VAX/DISP platform some time ago. Similarly, instead of using January and February 1997 as a test period, we favoured using a much more recent model formulation, and have been archiving relevant model data in real time since January 2000. Archived forecasts go as far as the model runs, to T+144, and not T+48 as originally proposed. The thinking was that any systematic errors implicit in the model formulation would grow with integration time, and thus should be easier to identify at longer lead times. One slight disadvantage of this is that because of space and time constraints a higher temporal resolution at short lead times has been lost, archived model data being 12-hourly, and database data currently 24-hourly.

A number of technical changes have been made since Hewson (1998b):

(i) Barotropic lows

Initially the database definition had included only frontal waves and potential waves (Table 1 and Figure 1). A new, third type of cyclonic feature, which we call the ‘barotropic low’, has now been incorporated. This was to capture apparently significant cyclonic features which were being missed by the frontal wave and potential wave definitions. Such lows are generally one of two types. Either they are cyclones not associated with a low level thermal gradient in their incipient stages (quite rare, but corresponds to the new type ‘C’ cyclone described in Deveson (2000) and Deveson et al (2001)), or, more commonly, they have evolved, during their life-cycle, from having a baroclinic structure to having a barotropic structure. In the latter case the life-cycle will often undergo the following transitions:

However note that occasional transitions from right to left in this sequence are also seen, particularly from frontal wave back to potential wave.

Barotropic lows are identified with the same methodology that we use to pinpoint the tips of potential waves and frontal waves (see Hewson (1997 and 1998a)), that is using pre-defined locating and masking diagnostics. The new diagnostics for barotropic lows are detailed in Table 1: essentially we pick out barotropic lows at the intersection points of zero contours of two orthogonal grid-relative 1000mb geopotential height gradient (or equivalently pressure gradient) components (locating equations BL1 and BL2). The masking diagnostics BM1 and BM2 are required because intersection points occur also in high centres and cols. BM2 represents the product of two second derivatives of the height field, which are respectively computed parallel to and perpendicular to the mean pressure gradient axis orientation in the vicinity (see Hewson(1998a) for a distinction between mean axes and mean vectors). The main distinguishing feature of a col is that the field curvatures in such suitably selected orthogonal directions are of opposite sign. In highs and lows they will be of the same sign. Thus mask BM2 can accurately remove all col points. Highs are then removed using the other masking quantity (BM1) which is proportional to geostrophic relative vorticity. Filtering applied to this field ensures we don't identify small multiple weak centres in areas of generally slack pressure gradient. Trial and error enabled the BM1 threshold to be set to an appropriate value.

(ii) Modifications to defining equations

The equation sets defining both frontal waves and potential waves have been extended slightly beyond those given in Hewson (1998b). The full new set, for all cyclone types, is given in Table 1. There are three key changes. Firstly an additional mask (WM3 and PM3), based on the cross-front rate of change of theta gradient (as opposed to theta-w), has been added to try to ensure that by using theta-w diagnostics to identify fronts we are not occasionally just picking up marked humidity discontinuities, and similarly to try also to exclude most 'warm conveyor belt fronts' (see Hewson (1998a)) from the analysis. Secondly, another simple mask (WM4 and PM4) was added to help reduce the proliferation of waves in the middle of anticyclonic regions (typically observed around the Mediterranean), where cross-front geostrophic winds occasionally exhibited slight positive vorticity, sometimes because of orographic influences, despite the fact that overall the relative vorticity was negative. The third change is in the threshold value used for mask PM6, the vorticity of the cross-front geostrophic wind. Originally the intention had been to capture every conceivable potential wave, from the very earliest stages, by setting this threshold to zero. However in practice the proliferation of potential waves became overwhelming, and a more pragmatic approach was adopted, which entailed increasing the threshold until we retained only potential waves which visibly had a clear link with some weakness in the background pressure pattern (which relates directly to low level geostrophic wind). Thus, as with most of the threshold values, some subjectivity is involved. This is a necessary step.

(iii) Clustering

When the locating contours for a particular type of feature are *nearly parallel*, several separate but closely-spaced intersection points can occur in one line. If represented as separate cyclonic features, these would be of dubious validity, given that the minimum number of gridlengths required, mathematically, to represent one cyclonic feature (i.e. a wavelength of a simple sine wave) is 4. On the raw GM grid 4 wavelengths total about 240km – so the model could not be expected to pick up waves with a separation smaller than this. Indeed the true threshold for reasonable representation is probably higher. A simple 'clustering' algorithm addresses this problem. Beginning with a screen dump of the isolated contour intersection pixels, we compute a 2-D matrix containing separations for every possible pixel pair combination. Then for the pair with the smallest separation we delete both pixels, but introduce a new pixel half way between. Relevant elements of the matrix are then re-computed, before again finding the smallest separation, and again combining those next two pixels into one at their mid point. This procedure continues until the minimum separation found exceeds a pre-defined threshold value. This has been set to 300km, to correspond to just over 4 model gridlengths. The impact this algorithm has on a pre-existing 'line' of wave/low pixels, is to re-organise them into points having a spacing typically just over 300km.

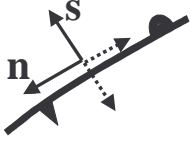
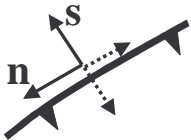
CYCLONIC FEATURE	DIAGNOSTIC TYPE	EQUATION	THRESH	COMMENTS
			-OLDS	
			<u>Standard</u> <u>Weak</u>	
FRONTAL WAVE <i>'A meeting point of cold and warm fronts at which the vorticity of the cross-front geostrophic wind is positive'</i> All variables are on the surface 'geopotential height above topography = 1km'  $\hat{s} = \pm \nabla \nabla \theta_w / \nabla \nabla \theta_w $ (5 point mean axis)	Locating Eqn. WL1	$\partial(\nabla \nabla \theta_w)_s / \partial s = 0$	-	Front locator
	Locating Eqn. WL2	$\mathbf{V}_G \cdot \nabla \theta_w = 0$	-	Zero geostrophic theta-w advection
	Masking Eqn. WM1	$-\nabla \nabla \theta_w \cdot \nabla \theta_w / \nabla \theta_w >$	$0.52 \text{ }^\circ\text{C} / (100\text{km})^2$ $0.26 \text{ }^\circ\text{C} / (100\text{km})^2$	Rate of change of theta-w gradient, across theta-w isotherms
	Masking Eqn. WM2	$ \nabla \theta_w + m\chi \nabla \nabla \theta_w >$	$1.17 \text{ }^\circ\text{C} / 100\text{km}$ $0.595 \text{ }^\circ\text{C} / 100\text{km}$	Approximate theta-w gradient in the adjacent baroclinic zone
	Masking Eqn. WM3	$-\nabla \nabla \theta \cdot \nabla \theta / \nabla \theta >$	$0.52 \text{ }^\circ\text{C} / (100\text{km})^2$ $0.26 \text{ }^\circ\text{C} / (100\text{km})^2$	Rate of change of theta gradient, across theta isotherms
	Masking Eqn. WM4	$\partial v / \partial x - \partial u / \partial y >$	0	Relative vorticity
	Masking Eqn. WM5	$[\nabla \nabla \theta_w \times \hat{k}] \cdot \nabla [-\mathbf{V}_G \cdot \nabla \tau] >$	0	Wave – anti-wave discriminant
POTENTIAL WAVE <i>'A point on a front characterised by a local maximum, in the along-front direction, in the vorticity of the cross-front geostrophic wind'</i> All variables are on the surface 'geopotential height above topography = 1km'  $\hat{s} = \pm \nabla \nabla \theta_w / \nabla \nabla \theta_w $ (5 point mean axis)	Locating Eqn. PL1	$\partial(\nabla \nabla \theta_w)_s / \partial s = 0$	-	Front locator (same as WL1)
	Locating Eqn. PL2	$\partial^2 V_{Gs} / \partial n^2 = 0$	-	Turning points in an along-front profile of vorticity of the cross-front geostrophic wind
	Masking Eqn. PM1	$-\nabla \nabla \theta_w \cdot \nabla \theta_w / \nabla \theta_w >$	$0.52 \text{ }^\circ\text{C} / (100\text{km})^2$ $0.26 \text{ }^\circ\text{C} / (100\text{km})^2$	Same as WM1
	Masking Eqn. PM2	$ \nabla \theta_w + m\chi \nabla \nabla \theta_w >$	$1.17 \text{ }^\circ\text{C} / 100\text{km}$ $0.595 \text{ }^\circ\text{C} / 100\text{km}$	Same as WM2
	Masking Eqn. PM3	$-\nabla \nabla \theta \cdot \nabla \theta / \nabla \theta >$	$0.52 \text{ }^\circ\text{C} / (100\text{km})^2$ $0.26 \text{ }^\circ\text{C} / (100\text{km})^2$	Same as WM3
	Masking Eqn. PM4	$\partial v / \partial x - \partial u / \partial y >$	0	Same as WM4
	Masking Eqn. PM5	$-\partial^3 V_{Gs} / \partial n^3 >$	0	Nature of turning point in the along-front profile of vorticity of the cross-front geostrophic wind (cf PL2)
Masking Eqn. PM6	$-\partial V_{Gs} / \partial n >$	$8.0 \times 10^{-6} \text{ s}^{-1}$	Vorticity of the cross-front geostrophic wind	
'BAROTROPIC' LOW  $\hat{s} = \pm \nabla \phi_{1000} / \nabla \phi_{1000} $ (5 point mean axis)	Locating Eqn. BL1	$\partial \phi_{1000} / \partial x = 0$	-	x-component of the pressure gradient
	Locating Eqn. BL2	$\partial \phi_{1000} / \partial y = 0$	-	y-component of the pressure gradient
	Masking Eqn. BM1	$(\nabla^2 \phi_{1000})_{filtered} >$	$1.0 \times 10^{-9} \text{ m}^{-1}$	Geostrophic vorticity factor (1-2-1 filter applied 4 times)
	Masking Eqn. BM2	$\partial^2 \phi_{1000} / \partial n^2 * \partial^2 \phi_{1000} / \partial s^2 >$	0	Col point discriminant

Table 1. Defining equations for different cyclone types.

At 00Z on 30/10/2000, from 00Z on 30/10/2000

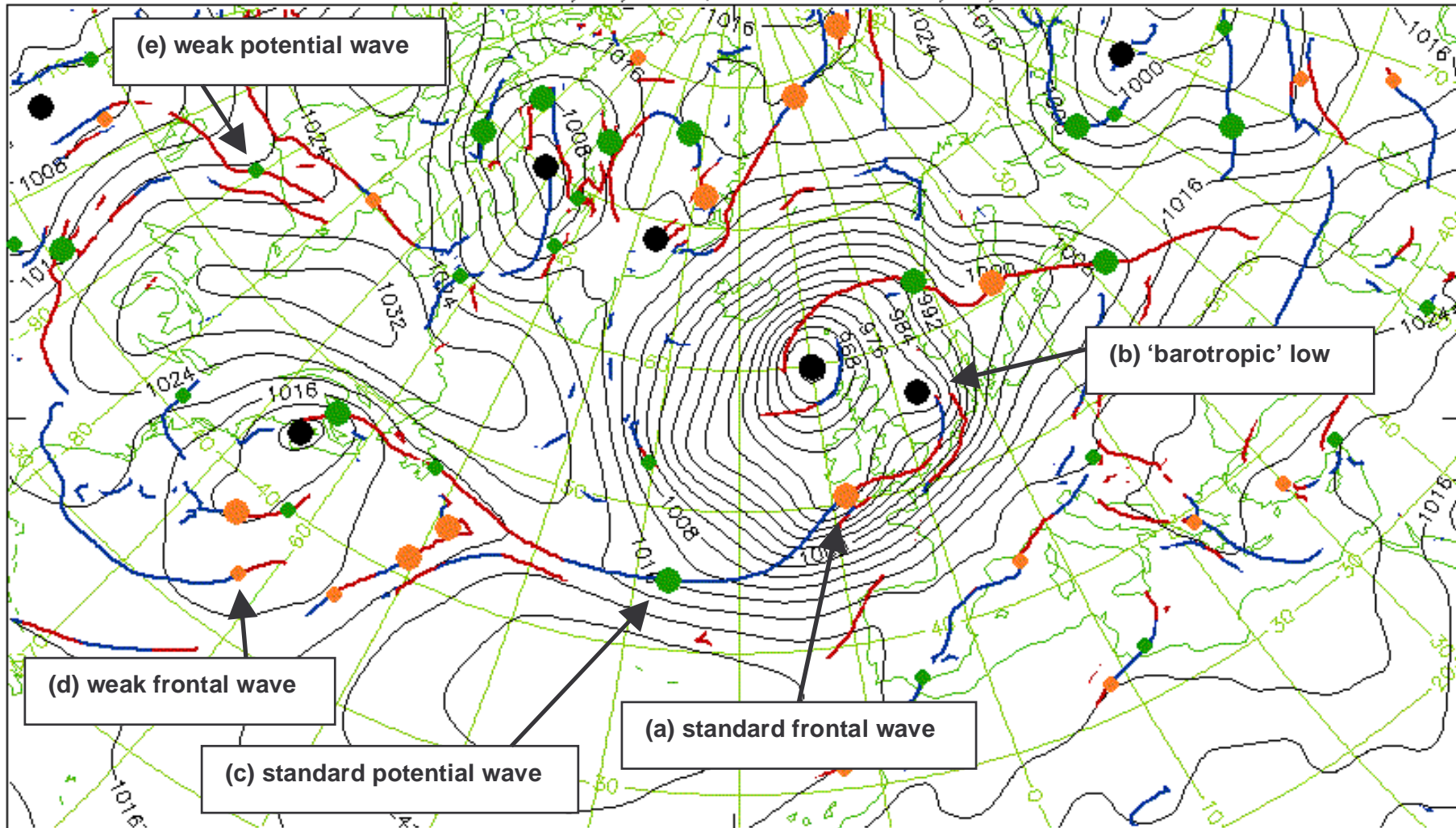


Figure 1: Standard and weak warm and cold objective fronts are shown as red and blue lines, derived using the surface 'gptl ht. above orography = 1km'. Black contours show mslp at 4mb intervals. Each spot type represents a different type of cyclonic feature, as labelled. The five types were plotted according to the *hierarchy* (a),(b),(c),(d),(e), which means that a 'co-location mask', applied after plotting each type, precludes identification of any other cyclonic feature later in the list within a 300km radius. Similarly, any two features of the same type closer than 300km initially will generally have been combined into one, located halfway between. Less reliance should be placed on any features over high topography

(iv) Hierarchies and co-location masking

Because the equation sets for the different cyclone types are not mutually exclusive, another problem similar to that addressed in (iii) is introduced: different types can be co-located. This necessitated introduction both of a plotting hierarchy, and of ‘co-location masking’. The 5 different categories of cyclonic disturbance have been assigned to the following hierarchy order (note that Table 1 lists the thresholds that distinguish ‘standard’ waves from ‘weak’ waves):

- (a) standard frontal waves
- (b) ‘barotropic’ lows
- (c) standard potential waves
- (d) weak frontal waves
- (e) weak potential waves

In practice any feature higher up the list takes priority. What this means, practically, is that we first identify type (a), standard frontal waves, at contour intersection points (and apply the clustering algorithm described in (ii)). Then we identify type (b), barotropic lows, and apply clustering. The wave co-location masking then deletes all the barotropic lows lying within a 300km radius of any of the previously identified standard frontal waves (type (a)). Next we identify type (c), the standard potential waves, and apply clustering, but subsequently also delete all of those that lie within a 300km radius of any remaining type (b) or type (a) features. And so the process continues. In this way no two cyclonic disturbances identified on one time frame should ever be closer than about 300km. The co-location masking thus prevents ‘double counting’. Hewson (1998) had suggested that diagnostic(s) could be used to perform the masking – in practice that approach proved less robust. Figure 1 shows the five cyclone types, during a stormy spell over the UK.

(v) Filtering

Noise in basic variable input fields is removed using a simple 1-2-1 filter, applied 10 times. Such a filter had been recommended as suitable for most purposes (Mike Pedder, JCOMM, Reading, personal communication). In tests applying the filter 10 times gave the optimum compromise between removing as many of the apparently spurious waves and potential waves as possible – which were often tied to orographic features, whilst at the same time retaining the vast majority of those waves which had coherent dynamical structures, and which forecasters would, subjectively, have interpreted as significant perturbations. A cusp had been evident on plots of ‘number of waves’ versus ‘filtering frequency f ’, at a value $f \approx 10$. No filtering is applied to the diagnostics themselves, only the input variables.

(vi) Geostrophic rate of Occlusion

The equation for the geostrophic rate of occlusion, γ_G , given in Hewson (1998b), has been revised to:

$$\gamma_G = \frac{-\pi}{2n} \sum_{i=1}^n \frac{1}{r_i} \text{SIGN} \left[\mathbf{r}_i \cdot (\hat{\mathbf{s}} \times \hat{\mathbf{k}}) \right] \left(\mathbf{V}_{Gsi} \cdot (\hat{\mathbf{r}}_i \times \hat{\mathbf{k}}) \right)$$

This new form allows also for computation around a ‘ring’ of n points which are approximately, but not exactly, equidistant from the central point. The radius vector \mathbf{r}_i represents a displacement from the central point out to the point in the ring, whilst $\hat{\mathbf{s}}$ is the cross-front unit vector, pointing towards cold air (see also Fig A4.1 in Hewson (1998b)). This diagnostic is of particular importance because it determines whether a wave is a cold front wave or a warm front wave, as indicated in Table 2 (updated from Hewson (1998b)).

	Warm Front Wave	Cold Front Wave
Potential (Frontal) Wave	Geostrophic thermal advection at wave tip is positive	Geostrophic thermal advection at wave tip is negative
Frontal Wave	Geostrophic rate of occlusion, at a radius $r \approx 200\text{km}$, is negative	Geostrophic rate of occlusion, at a radius $r \approx 200\text{km}$, is positive

Table 2. Wave type identification methods

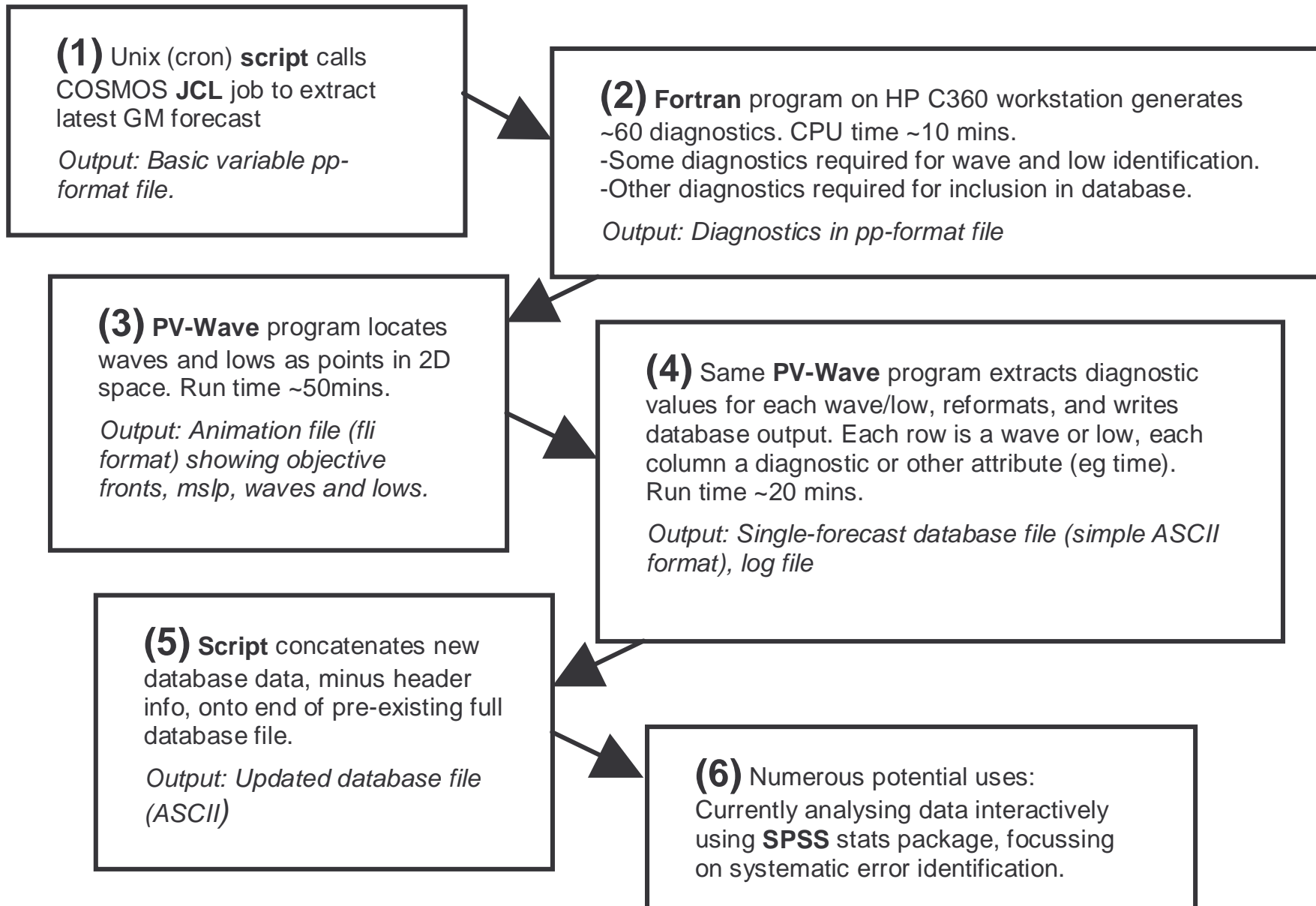


Figure 2. Stages in database construction.

1.2 Data Processing

The flow chart in Figure 2 shows how the cyclone database is updated with new data. Bold text shows the software types in use at each stage. Run times are given as an approximate guide, and relate only to the current program structure, with the areas, levels and times as described below. To process data covering the whole globe would take much longer.

Below we elaborate on processing currently performed at each stage:

- (1) Data is extracted (by interpolation) onto an equivalent of the old LAM area, with its rotated pole lat/long grid (as shown, for example, in Figure 1). The rotated grid gridpoint separation is 0.4425 degrees ($\approx 50\text{km}$) in both latitude and longitude. All the basic variables ϕ , u , v , T , RH and ω are downloaded, on all model levels, at 12 hour intervals from $T+0$ to $T+144$, for the 00Z GM forecast only.
- (2) The Fortran diagnostics program first interpolates the model level data onto 100hPa interval pressure levels, from 1000hPa to 100hPa. Then wind vector component pairs are re-projected to be relative to the rotated grid. Next the filtering is applied, as described above in section 1.1(v). Finally the required diagnostics are computed from the filtered data, mostly using simple finite differencing. Panagi and Dicks (1997) give an overview of the diagnostics suite utilised; additional variables developed for this project are documented here, in Hewson (1997, 1998a, 1998b) and in Renfrew et al (1997).
- (3) A 5000 line PV-Wave program processes, graphically, at each forecast lead time, those diagnostics required for the identification of each wave type. The primary functions used are contouring and colour-filling, as described in Hewson (1998a). For identification of waves and potential waves the level used is the ‘geopotential height above orography = 1km’ surface. The PV-Wave program interpolates diagnostics from pressure levels onto this surface before plotting proceeds. The program also performs the clustering and co-location masking described above in sections 1.1(iii) and 1.1(iv).
- (4) The PV-Wave program is designed to extract and output diagnostic and other data, from the GM output file produced at stage (2), in about 4 different ways:
 - (a) peripheral data, such as date and lead time, taken from file headers or hardwired in
 - (b) diagnostic data extracted *at* the wave/low locations, from the appropriate pressure level(s) in the current file, or in a corresponding ‘land surface’ file (mainly used for SSTs).
 - (c) diagnostic data extracted *around* the wave/low locations, by searching within pre-defined radii of 300km or 600km, for a maximum or minimum value. Implicit in the search is the idea that it one can *attribute* or *link* such a value to the cyclonic feature in question. This type of diagnostic was not incorporated in Hewson (1998). The need arose from the desire to investigate, for example, the wind speed maxima that are typically found around intense cyclones. Most such diagnostics are accompanied by supporting values, to inform the database user of the location, relative to the cyclonic disturbance, of the extrema.
 - (d) diagnostic values that have to be *recomputed* from the input diagnostics, making some assumptions (these are highlighted in bold in the database variable table, and due to complexity and time constraints are not currently operational).
- (5) All the cyclone database files - that is the small ‘one-forecast’ files, as well as the complete database - are written with the same simple spreadsheet structure, described below in section 2.1.
- (6) Results from initial analysis of about one year’s worth of data are presented in section 4.

2. Database Content

2.1 Structure

The database has been structured in a convenient, compact ASCII spreadsheet format, to ease cross-platform transfer, and minimise space requirements.

Each row (except the first) corresponds to a cyclonic disturbance, and each item in the row an attribute (e.g. diagnostic) for that disturbance. The data is comma-delimited, missing values being indicated by the MDI entry 99999, except for model omega values (beyond $T+48$) for which the MDI is -2147483648.

The first row in the database contains comma-delimited character string column headings, each no more than 8 characters in length, which describe the variables the columns represent. These are listed in the database variable table (Table 3).

Each variable has a numeric, character or date format. Character variables are of a pre-defined length (1 to 8) that is specific to a column. All numeric variables have been converted to integer form, by multiplication of SI unit values by a scaling factor suitable for representing characteristic value ranges, typically, with 3 digit precision.

2.2 Variables

Table 3 lists all the diagnostics currently built into the database, giving, for each, the column heading variable name, information on any changes incorporated since Hewson (1998b), variable type, units information and the inverse scaling factor, and finally an indication of current status, together with estimates of work required and priority levels for the few variables for which only MDIs are currently stored.

2.3 Data Coverage

For various technical reasons some data is missing from the database. Table 4 shows which of the 00Z GM forecasts have been missed, and why.

2.4 Statistics and Hints for Data Reduction

The current cyclone database contains about 100,000 lines of data, and occupies about 60Mbytes. This includes about 300 days worth of 00Z GM forecast runs, with data at 24 hour intervals from T+0 through to T+144. Typically about 60 cyclonic disturbances are identified on each time frame, which corresponds, on average, to just over one for every other $10^{\circ} \times 10^{\circ}$ lat/long box. Running through stages (2) to (5) on figure 2 for all 300 forecasts took about 10 days, as sole user on one HP C360 workstation. Input data, which had been archived in real time on optical disk, as the output of stage 1, was downloaded, typically, in 2 month blocks. 2 months corresponds to about 12 Gbytes of input data.

Common problems encountered when analysing large databases with, say, a statistical package, are an inability to load the data and slow processing of queries and plot requests. There are a number of ways to circumvent such problems, which mainly involve data reduction; by row, by column, or by both:

Rows: Studies of limited periods – say for a particular month – can be conducted by concatenating together ‘one-forecast’ files, using the unix command ‘tail +1’ to remove superfluous header information from all but the first file.

Columns: For studies of particular aspects of cyclone structure columns can be removed using the versatile unix ‘cut’ command, with the comma delimiter defined.

Standard statistical package facilities can also reduce the database size.

Var No.	Column Heading (= variable name)	Changes since previous report ?	Standard Symbol	Description	Var Type	Units, or type of character variable†	Scaling Factor (to multiply data by to give quoted units)	Current Status (prior=H,M,L / time est ~ Month, Week, Day)
1	Model	No	-	Version of Met Office Unified Model	C*2	†e.g. G1	-	✓
2	Region	was C*2	-	Region used in frontal wave analysis	C*3	†e.g. LA1	-	✓
3	Resoln	No	-	Typical horizontal resolution of input data	N	Km	1	✓
4	ProjWind	No	-	Projection information for interpreting vector and other 'x' and 'y' components	C*6	†e.g. ELL-TP	-	✓
5	AnDate	No	DT	Date of analysis	D	dd/mm/yy	-	✓
6	AnWkDay	was C*2	-	Day of week for analysis	C*3	†e.g. MON	-	✓
7	AnTime	No	DT	Time of analysis	N	Hrs	1	✓
8	AcDate	No	VT	Validating date of data	D	dd/mm/yy	-	✓
9	AcWkDay	was C*2	-	Validating day of week of data	C*3	†e.g. MON	-	✓
10	AcTime	No	VT	Validating time of data	N	Hrs	1	✓
11	LeadTime	No	-	Difference of forecast time from analysis time (total hrs)	N	Hrs	1	✓
12	Lat	No	ϕ	Latitude of frontal wave (+=N)	N	Deg	0.1	✓
13	Lon	No	λ	Longitude of frontal wave (+=E)	N	Deg	0.1	✓
14	WavType	'L' added	-	Actual frontal wave, or Potential wave, or barotropic Low (section 1.1(i) above)	C*1	†A, P or L	-	✓
15	WavStren	'L' added	-	Standard wave, Weak wave or barotropic Low (section 1.1(iv) above)	C*1	†S, W or L	-	✓
16	WavErr	No	$\delta\epsilon_{wave}$	Frontal wave location error (in Hewson(1997))	N	km	1	L / W-
17	WavFType	'L' added	-	Warm front wave, or Cold front wave, or barotropic Low (section 1.1(vi) above)	C*1	†W, C or L	-	✓
18	MSLP	No	P	Mean sea level pressure	N	hPa	0.1	✓
19	MSLPtype	No	-	Raw MSLP or derived from 1000mb height?	C*1	†R or H	-	✓
20	RVor1	No	ζ	Relative Vorticity at 1km	N	s ⁻¹	10 ⁻⁶	✓
21	RVor1XF	No	ζ_{xf}	Relative vorticity of the cross-front wind at 1km	N	s ⁻¹	10 ⁻⁶	M / D-
22	RVor1LF	No	ζ_{lf}	Relative vorticity of the along-front wind at 1km	N	s ⁻¹	10 ⁻⁶	M / D-
23	GRVor1	No	ζ_G	Geostrophic Relative Vorticity at 1km	N	s ⁻¹	10 ⁻⁶	✓
24	GRVor1XF	No	ζ_{xfG}	Relative vorticity of the cross-front geostrophic wind at 1km	N	s ⁻¹	10 ⁻⁶	✓
25	GRVor1LF	No	ζ_{lfG}	Relative vorticity of the along-front geostrophic wind at 1km	N	s ⁻¹	10 ⁻⁶	✓
26	FX	No	n_x	x-component of the along-front unit vector	N	-	0.01	H / D-
27	FY	No	n_y	y-component of the along-front unit vector	N	-	0.01	H / D-
28	Te9	No	T	Temperature at 900mb	N	°C	0.1	✓
29	ThW9	No	θ_{W900}	Theta-W at 900mb	N	°C	0.1	✓

30	ThW7	No	θ_{W700}	Theta-W at 700mb	N	°C	0.1	✓
31	ThW5	No	θ_{W500}	Theta-W at 500mb	N	°C	0.1	✓
32	Th9	No	θ_{900}	Potential Temperature at 900mb	N	°C	0.1	✓
33	Th7	No	θ_{700}	Potential Temperature at 700mb	N	°C	0.1	✓
34	Th5	No	θ_{500}	Potential Temperature at 500mb	N	°C	0.1	✓
35	ABZGrThW	No	$ \nabla\theta_w _{ABZ}$	Theta-W gradient in the adjacent baroclinic zone at 1km	N	°C/km	10^{-4}	✓
36	AFGrThW	No	$\nabla\theta_w \cdot \hat{n}$	Along-front Theta-W gradient at 1km	N	°C/km	10^{-4}	H / D
37	Fr600ThW	No	<small>≡ diagnostic WL1 in Table 1 (at 600mb)</small>	Value of Theta-W front locating diagnostic at 600mb	N	°C/Km ³	10^{-8}	✓
38	GThWAdv6	No	$-\mathbf{V}_G \cdot \nabla\theta_w$	Geostrophic advection of Theta-W at 600mb	N	°C/s	10^{-6}	✓
39	ABZGrTh	No	$ \nabla\theta _{ABZ}$	Theta gradient in the adjacent baroclinic zone at 1km	N	°C/km	10^{-4}	✓
40	AFGrTh	No	$\nabla\theta \cdot \hat{n}$	Along-front Theta gradient at 1km	N	°C/km	10^{-4}	H / D
41	Fr600Th	No	<small>≡ diagnostic WL1 in Table 1 (at 600mb, θ not θ_w)</small>	Value of Theta front locating diagnostic at 600mb	N	°C/km ³	10^{-8}	✓
42	GThAdv6	No	$-\mathbf{V}_G \cdot \nabla\theta$	Geostrophic advection of Theta at 600mb	N	°C/s	10^{-6}	✓
43	U7	no longer grid-relative	U_{700}	U Component at 700mb (WE)	N	m/s	0.1	✓
44	V7	no longer grid-relative	V_{700}	V component at 700mb (SN)	N	m/s	0.1	✓
45	U5	no longer grid-relative	U_{500}	U Component at 500mb (WE)	N	m/s	0.1	✓
46	V5	no longer grid-relative	V_{500}	V component at 500mb (SN)	N	m/s	0.1	✓
47	U3	no longer grid-relative	U_{300}	U Component at 300mb (WE)	N	m/s	0.1	✓
48	V3	no longer grid-relative	V_{300}	V component at 300mb (SN)	N	m/s	0.1	✓
49	PV1km	No	-	PV at 1km	N	PVunits	0.01	✓
50	PV2ht	No	-	Height of PV2 surface (scan down)	N	dm	1	✓
51	PVfold	No	-	Whether fold exists in surface of PV=1.5 PV units	C*1	Y or N	-	M / W
52	W9	No	ω_{900}	Model Vertical velocity at 900mb	N	cm/s	0.01	✓ (to T+48)
53	W7	No	ω_{700}	Model Vertical velocity at 700mb	N	cm/s	0.01	✓ (to T+48)
54	W5	No	ω_{500}	Model Vertical velocity at 500mb	N	cm/s	0.01	✓ (to T+48)
55	Div1000	No	$\nabla \cdot \mathbf{V}_{1000}$	Divergence at 1000mb	N	s ⁻¹	10^{-7}	✓
56	Div900	No	$\nabla \cdot \mathbf{V}_{900}$	Divergence at 900mb	N	s ⁻¹	10^{-7}	✓
57	Div800	No	$\nabla \cdot \mathbf{V}_{800}$	Divergence at 800mb	N	s ⁻¹	10^{-7}	✓
58	Div500	No	$\nabla \cdot \mathbf{V}_{500}$	Divergence at 500mb	N	s ⁻¹	10^{-7}	✓
59	Div300	No	$\nabla \cdot \mathbf{V}_{300}$	Divergence at 300mb	N	s ⁻¹	10^{-7}	✓
60	LandSea	No	-	Whether nearest gridpoint is land or sea	C*1	†L or S	-	✓
61	SeaGrPts	No	-	Number of the 9 adjacent gridpoints which are sea	N	-	1	BUG H / D
62	SST	MDI used over land / ice	T_{sea}	Sea surface temperature at nearest grid point (or MDI if land or >0.5 sea ice)	N	°C	0.1	✓

63	GrSST	MDI used for land / ice	$ \nabla T_{\text{sea}} $	Sea surface temperature gradient (or MDI if any gridpoints with land or >0.5 sea ice required for computation)	N	°C/km	10^{-4}	✓
64	GrSSTx	MDI used for land / ice	$\partial T_{\text{sea}} / \partial x$	'X'-cpt of Sea surface temperature gradient (or MDI if any gridpoints with land or >0.5 sea ice required for computation)	N	°C/km	10^{-4}	✓
65	GrSSTy	MDI used for land / ice	$\partial T_{\text{sea}} / \partial y$	'Y'-cpt of Sea surface temperature gradient (or MDI if any gridpoints with land or >0.5 sea ice required for computation)	N	°C/km	10^{-4}	✓
66	AlphaMin	No	α_{min}	Critical environmental strain threshold	N	s^{-1}	10^{-7}	M / M+
67	VortMeth	No	-	Method by which vorticity values (eg: vars 20-22) were calculated	C*6	†e.g. O1CFLG	-	✓
68	UE	No	U_E	U Cpt of the 'environmental' wind	N	m/s	0.1	M / M+
69	VE	No	V_E	V Cpt of the 'environmental' wind	N	m/s	0.1	M / M+
70	dVEdS	No	$\partial V_{E_s} / \partial s$	Rate of change of front-normal cpt of the 'environmental' wind in a front-normal dirn	N	s^{-1}	10^{-7}	M / M+
71	dVEdN	No	$\partial V_{E_s} / \partial n$	Rate of change of front-normal cpt of the 'environmental' wind in a front-parallel dirn	N	s^{-1}	10^{-7}	M / M+
72	RH9	No	-	Relative humidity w.r.t. ice at 900mb	N	%	0.1	✓
73	RH7	No	-	Relative humidity w.r.t. ice at 700mb	N	%	0.1	✓
74	RH5	No	-	Relative humidity w.r.t. ice at 500mb	N	%	0.1	✓
75	WQGT7	No	ω_{qg7}	Vertical velocity at 700mb attributable to q-g forcing	N	cm/s	0.01	✓
76	WQGU7	No	ω_{qgu7}	Vertical velocity at 700mb attributable to q-g forcing above 650mb	N	cm/s	0.01	✓
77	WQGM7	No	ω_{qgm7}	Vertical velocity at 700mb attributable to q-g forcing between 850mb and 550mb	N	cm/s	0.01	✓
78	WQGL7	No	ω_{qgl7}	Vertical velocity at 700mb attributable to q-g forcing below 750mb	N	cm/s	0.01	✓
79	THIKN05	No	Z_T	1000-500mb thickness	N	dm	0.1	✓
80	ShRVort3	No	ζ_{sh}	Shear relative vorticity at 300mb	N	s^{-1}	10^{-6}	✓
81	GOcRate1	Small mods to code & n=12 instead of 4	γ_G	Geostrophic rate of occlusion at 1km; n=12, R~100km (section 1.1(vi) above)	N	s^{-1}	10^{-7}	✓
82	GOcRate2	Small mods to code & n=24 instead of 4	γ_G	Geostrophic rate of occlusion at 1km; n=24, R~200km (section 1.1(vi) above)	N	s^{-1}	10^{-7}	✓
83	AcDay	changed from analysis to actual	-	Validating Date (day)	N	-	1	✓
84	AcMonth	changed from analysis to actual	-	Validating Month	N	-	1	✓
85	AcYear	changed from analysis to actual	-	Validating Year (4 DIGIT)	N	-	1	✓
86	Vmax@9R3	New	$ U_{\text{max}} $	Maximum wind strength, at 1km, within a 300km radius	N	m/s	0.1	✓
87	u@Vm9R3	New	u	U component (EW) of the maximum wind vector in var 86	N	m/s	0.1	✓
88	v@Vm9R3	New	v	V component (SN) of the maximum wind vector in var 86	N	m/s	0.1	✓
89	dx@Vm9R3	New	δx	Displacement in EW direction of the maximum wind vector in var 86	N	km	1	✓
90	dy@Vm9R3	New	δy	Displacement in SN direction of the maximum wind vector in var 86	N	km	1	✓

91	dr@Vm9R3	New	δr	Radial displacement of the maximum wind vector in var 86	N	km	1	✓
92	Vmax@9R6	New	$ \mathbf{U}_{\max} $	Maximum wind strength, at 1km, within a 600km radius	N	m/s	0.1	✓
93	u@Vm9R6	New	u	U component (EW) of the maximum wind vector in var 92	N	m/s	0.1	✓
94	v@Vm9R6	New	v	V component (SN) of the maximum wind vector in var 92	N	m/s	0.1	✓
95	dx@Vm9R6	New	δx	Displacement in EW direction of the maximum wind vector in var 92	N	km	1	✓
96	dy@Vm9R6	New	δy	Displacement in SN direction of the maximum wind vector in var 92	N	km	1	✓
97	dr@Vm9R6	New	δr	Radial displacement of the maximum wind vector in var 92	N	km	1	✓
98	Vmax@3R3	New	$ \mathbf{U}_{\max} $	Maximum wind strength, at 300mb, within a 300km radius	N	m/s	0.1	✓
99	u@Vm3R3	New	u	U component (EW) of the maximum wind vector in var 98	N	m/s	0.1	✓
100	v@Vm3R3	New	v	V component (SN) of the maximum wind vector in var 98	N	m/s	0.1	✓
101	dx@Vm3R3	New	δx	Displacement in EW direction of the maximum wind vector in var 98	N	km	1	✓
102	dy@Vm3R3	New	δy	Displacement in SN direction of the maximum wind vector in var 98	N	km	1	✓
103	dr@Vm3R3	New	δr	Radial displacement of the maximum wind vector in var 98	N	km	1	✓
104	Vmax@3R6	New	$ \mathbf{U}_{\max} $	Maximum wind strength, at 300mb, within a 600km radius	N	m/s	0.1	✓
105	u@Vm3R6	New	u	U component (EW) of the maximum wind vector in var 104	N	m/s	0.1	✓
106	v@Vm3R6	New	v	V component (SN) of the maximum wind vector in var 104	N	m/s	0.1	✓
107	dx@Vm3R6	New	δx	Displacement in EW direction of the maximum wind vector in var 104	N	km	1	✓
108	dy@Vm3R6	New	δy	Displacement in SN direction of the maximum wind vector in var 104	N	km	1	✓
109	dr@Vm3R6	New	δr	Radial displacement of the maximum wind vector in var 104	N	km	1	✓
110	QTr3max	New	$\omega_{qg7(\max)}$	Maximum value of vertical velocity at 700mb attributable to q-g forcing; detected within a 300km radius	N	cm/s	0.01	✓
111	QTr3mxdx	New	δx	Displacement in EW direction of the maximum value given in var 110	N	km	1	✓
112	QTr3mxdy	New	δy	Displacement in SN direction of the maximum value given in var 110	N	km	1	✓
113	QTr3mxdr	New	δr	Radial displacement of the maximum value given in var 110	N	km	1	✓
114	QTr3min	New	$\omega_{qg7(\min)}$	Minimum value of vertical velocity at 700mb attributable to q-g forcing; detected within a 300km radius	N	cm/s	0.01	✓
115	QTr3mndx	New	δx	Displacement in EW direction of the minimum value given in var 114	N	km	1	✓
116	QTr3mndy	New	δy	Displacement in SN direction of the minimum value given in var 114	N	km	1	✓
117	QTr3mndr	New	δr	Radial displacement of the minimum value given in var 114	N	km	1	✓
118	QUr6max	New	$\omega_{qu7(\max)}$	Maximum value of vertical velocity at 700mb attributable to q-g forcing above 650mb; detected within a 600km radius	N	cm/s	0.01	✓

119	QUr6min	New	$\omega_{qgu7(\min)}$	Minimum value of vertical velocity at 700mb, attributable to q-g forcing above 650mb; detected within a 600km radius	N	cm/s	0.01	✓
120	QLr3max	New	$\omega_{qgl7(\max)}$	Maximum value of vertical velocity at 700mb attributable to q-g forcing below 750mb; detected within a 300km radius	N	cm/s	0.01	✓
121	QLr3min	New	$\omega_{qgl7(\min)}$	Minimum value of vertical velocity at 700mb, attributable to q-g forcing below 750mb; detected within a 300km radius	N	cm/s	0.01	✓
122	QUdipole	New	-	Strength of upper level forcing dipole (average of the magnitudes of vars 118 and 119)	N	cm/s	0.01	✓
123	QLdipole	New	-	Strength of lower level forcing dipole (average of the magnitudes of vars 120 and 121)	N	cm/s	0.01	✓
124	GridLat	New	'y'	Grid-relative latitude	N	degrees	0.1	✓
125	GridLon	New	'x'	Grid-relative longitude	N	degrees	0.1	✓
126	y2kAnDT	New	YYYYMMDD	Analysis date in Y2K-compliant format	C*8	-	-	H / D-
127	y2kFcDT	New	YYYYMMDD	Validating date in Y2K-compliant format	C*8	-	-	H / D-

Table 3: List of variables.

3 Risk summary

Extraneous problems encountered in the course of the project are itemised below, in decreasing order of significance. A rough estimate of the number of ‘man weeks’ spent addressing these problems is also given. Numerous programming bugs were also introduced, and removed, by the present author in the course of the project!

- 1) Serious bug in the PV-Wave colour-filling facility, which randomly missed out some highs and lows. Solved in-house by PV-Wave support. 10 weeks.
- 2) Errors in COSMOS fieldsfile extraction programs for converting wind components into a different grid-relative form. Solved by performing the appropriate rotation within the project’s own FORTRAN diagnostic code. 4 weeks.
- 3) Miscellaneous bugs in some of the diagnostics code procured from Reading. 4 weeks.
- 4) Occasional problems with routine, real-time extraction of data from COSMOS, for various reasons (as itemised on Table 4). This had been expected. Ongoing, though situation has improved with help from UNIX support. 2 weeks.
- 5) Unable to run PV-wave code successfully in batch mode. Workaround used. Problem not yet solved.
- 6) Bug in all the Unified Model’s Sea Surface Temperature fields. SST depends strongly on the integer value of latitude. Not yet solved. On NWP fix list. 1 week.

4 Initial Analysis

As analysis has only just begun, only a few results are presented in this section.

4.1 Climatologies

Figures 3 and 4 illustrate some simple ‘climatological’ information generated from the cyclone database, using only T+0 data for cyclone types (a) and (b) – see Figure 1. It should be borne in mind that the year in question (2000) was unusually cyclonic over the UK, and there is probably a net south-eastward displacement, towards the UK, on Figure 3, of many of the features shown, relative to what one might have seen had data been composited over a much longer period. Nevertheless, to the author’s knowledge no comparable data on warm and cold front waves has been published before.

Figure 3 shows cold front waves scattered throughout the domain, albeit with very few at low latitudes. There are more in the west of the North Atlantic than in the east, albeit still with mini clusters southwest of the UK (somewhat surprisingly) and also just northwest of Iberia. Coastal regions such as near Baffin Island, off eastern Greenland, off northwest Norway, and in northern parts of the Mediterranean, and the Adriatic, all seem to favour the development of cold front waves. Warm front waves are somewhat less numerous, but show the same broad spatial distributions as the cold front waves. Notably, however, the maximum near to eastern Greenland is this time displaced well out over the ocean. Although further investigation is required, this may perhaps indicate that katabatic drainage of cold air off the east Greenland coast is an important mechanism for cold front wave formation in this region – note that the equation in section 1.1(vi) is essentially measuring whether cold or warm advection are dominant around a wave. Barotropic lows show a different overall distribution in the North Atlantic basin to the frontal waves; most are present on the eastern side, with relatively few in the west. Indeed there is a striking absence of such features near 45N 40W, indicating that differential sea surface fluxes in this area probably play a significant part in *maintaining* baroclinicity within any cyclonic features that do develop. The west to east shift in population between the waves and the barotropic lows is broadly consistent with storm track dynamics, in which the baroclinic energy present in the west Atlantic tends to convert to kinetic energy in the east Atlantic, within cyclonic features that at low levels at least have become thermally weak. The barotropic lows shown over Greenland and some other mountainous areas can not generally be relied upon, although those over Spain probably represent summertime heat lows.

Figure 4 shows the central pressure values, with a reduced North Atlantic domain, of all standard waves and barotropic lows identified at the standard 00Z analysis time. Relative to a normal distribution (curved line) the pattern is slightly skewed. Sub- 990, 980, 970, 960 and 950hPa lows constitute, respectively, 21, 10, 3.2, 0.9 and 0.1% of this population. The North Sea storm of 30th October 2000 (Hewson, 2001) ranks 3rd out of 1244 in the list, with a central pressure, at 00z on 31st, of 954hPa. The frontal wave shown just south of Ireland on Figure 1 is this storm during a period of rapid intensification. It is likely that more lows, including this one, would show up with sub-950hPa pressures had more than just one analysis per day been used, although there is no reason to expect that this would change the above percentages systematically.

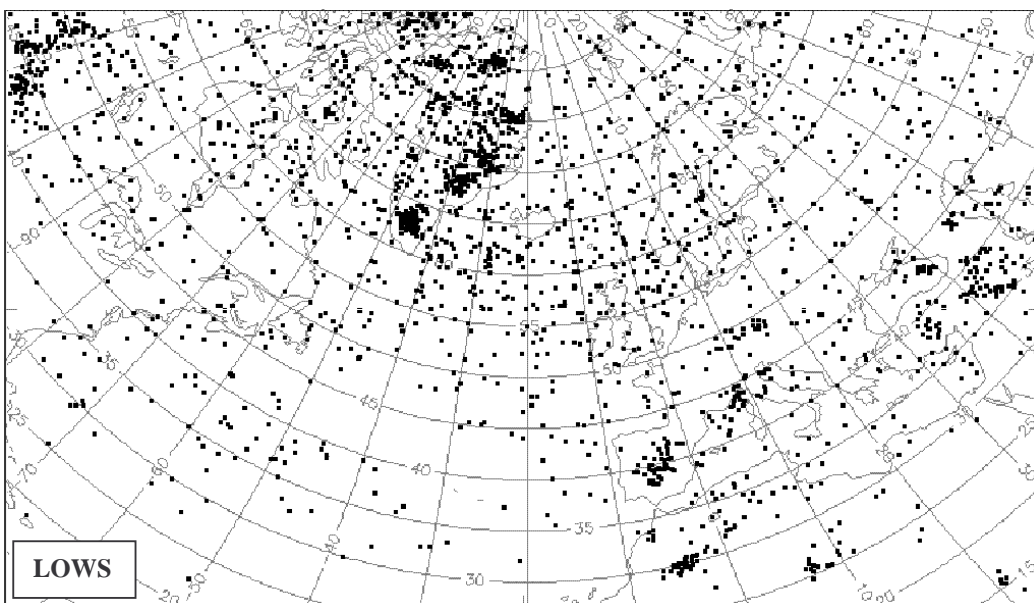
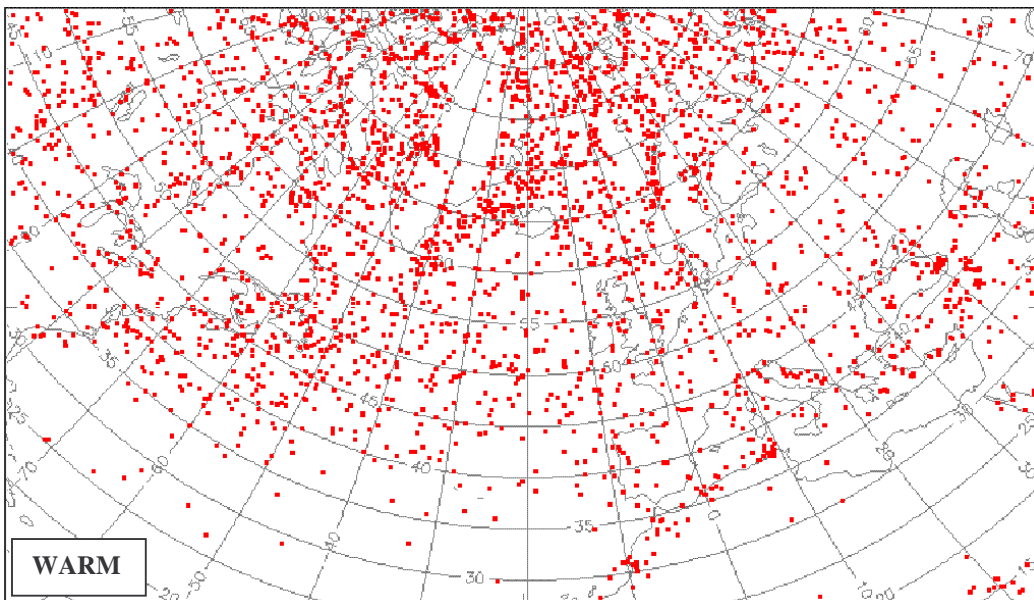
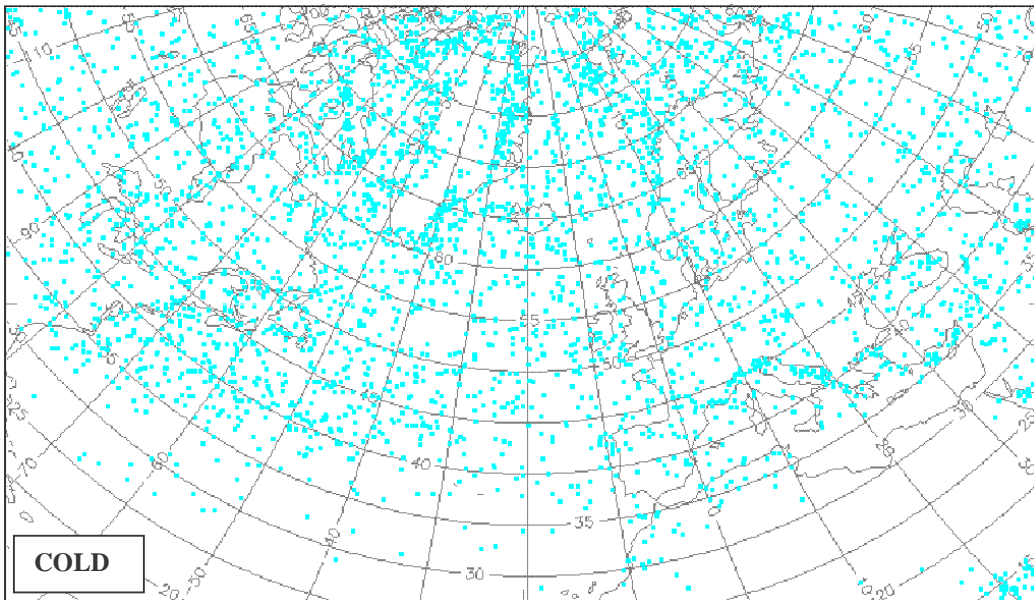
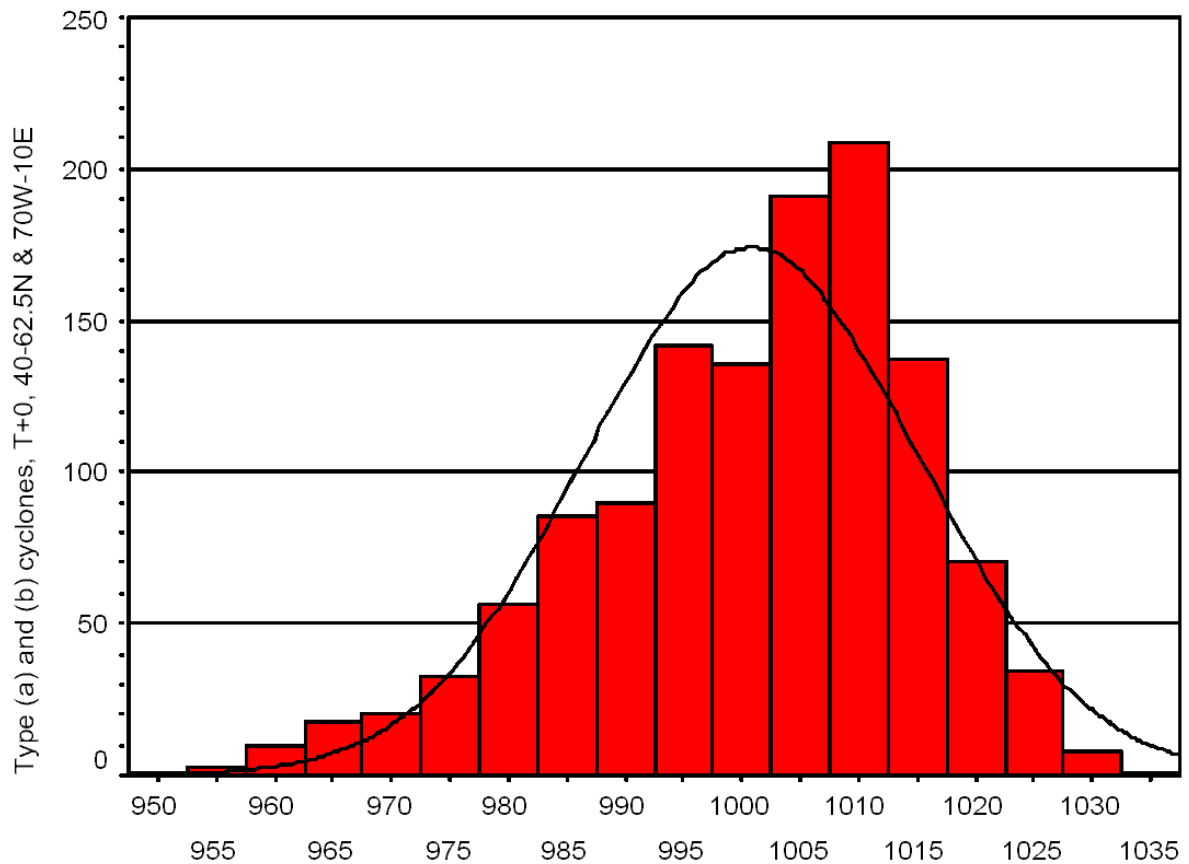


Figure 3: Year 2000 climatologies (from 00Z analyses) of cold front waves, warm front waves and barotropic lows (cyclone types (a) and (b) on Figure 1).



MSLP

Figure 4: Central pressure climatology, for 00Z analyses for 2000, showing total numbers of standard waves plus barotropic lows (cyclone types (a) and (b) on Figure 1) in a reduced North Atlantic domain of 40 to 62.5N, 70W to 10E.

4.2 Forecasting Aspects

Figure 5 compares, at different forecast lead times, for the year 2000 database, cyclone distributions categorised by the maximum model wind occurring within a 300km radius of each cyclone centre, at a geopotential height of 1km above the earth's surface (variable 86 in Table 3), for cyclone centres within the reduced North Atlantic domain referred to in Figure 4. This wind level should be a reasonable proxy for maximum surface gusts, so categorisation approximates, in one sense, to 'storm severity'. Encouragingly there appear to be no systematic biases at the more extreme end of the storm spectrum (say yellow through brown), with the populations in each category not, apparently, being a function of lead time (one caveat here is that the model's resolution may limit its ability to accurately replicate extreme winds, either in analyses or forecasts, and this will not show up in these plots). For more modest wind maxima, around 20m/s, there does appear to be a small shortfall in number of cyclones forecast.

Figure 6 shows the spatial distribution of 'modest cyclones' (wind maxima categories of 10,15 and 20 m/s) around the UK at T+0 and T+48. There appear to be insufficient standard frontal waves (red dots) forecast over northern France (lower right corner of plot), and insufficient barotropic lows (blue dots) around and west of the UK, although statistical testing is required to elucidate the significance of these observations. Other data (not shown) suggests a shortfall in forecast cold front waves over the area of large sea surface temperature gradients southwest of Newfoundland, and also suggests that in some areas the shortfall in frontal wave numbers may link to an over-abundance of potential waves. However all these initial impressions require further investigation.

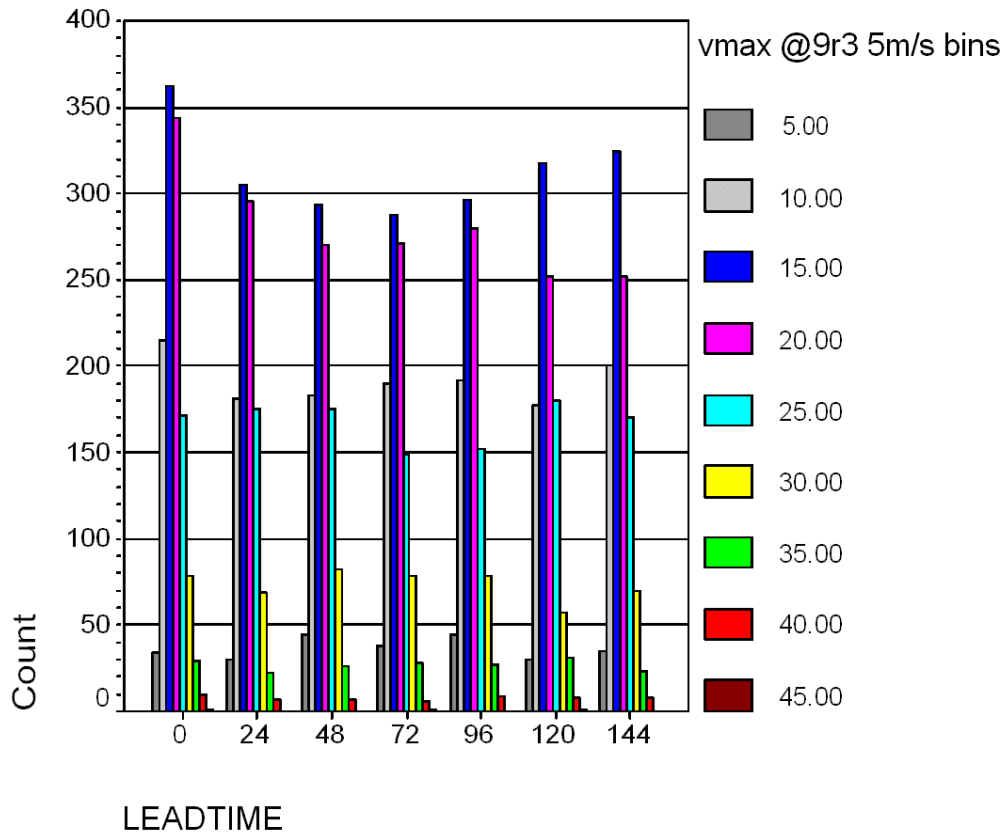


Figure 5: Spectra of the wind speed maxima present within a 300km radius of each frontal wave and barotropic low (types (a) and (b) on Figure 1), in 00Z GM analyses and forecasts during the year 2000.

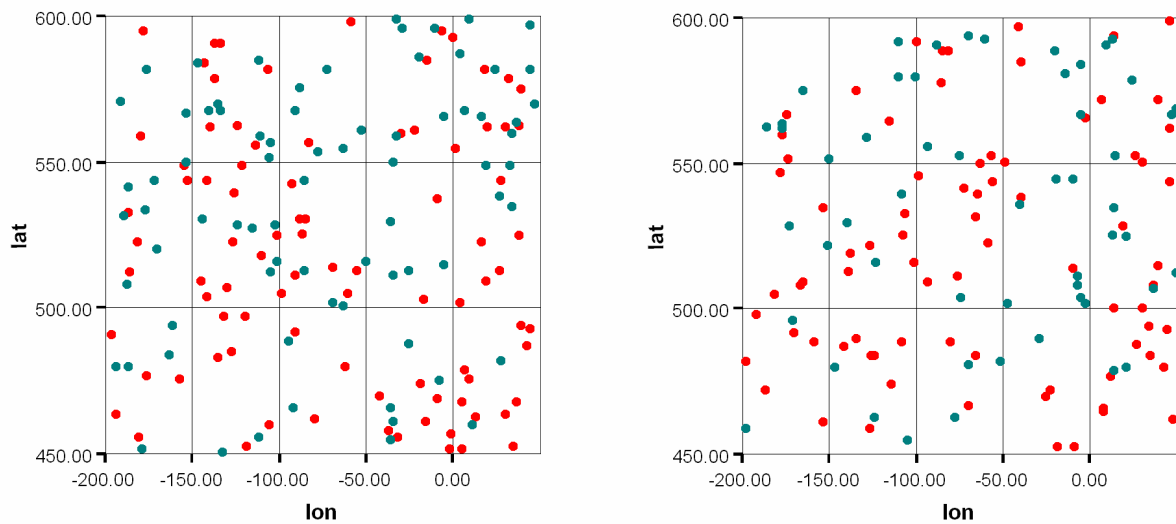


Figure 6: Locations of both standard frontal waves (red dots, type (a) on Figure 1) and barotropic lows (blue dots, type (b) on Figure 1) which are associated with modest low level wind speed maxima (10 to 20m/s, see Figure 5), in 00z GM analyses (left) and T+48 forecasts (right), for a reduced domain close to the UK. Divide plotted latitude and longitude values by 10.

5. Conclusions

- The concept of a cyclone database outlined in Hewson (1998b) has now been realised, albeit with a number of improvements
- Considerable effort has gone into developing the cyclone-locating methodology to the point where the results are both physically and synoptically meaningful. Previous formulations had identified far too many cyclonic features, most of which were unrealistic. Using various techniques including filtering, terrain following co-ordinates, clustering, cyclone hierarchies, extension of the defining equation sets and modifying masking thresholds this problem has essentially been solved. However in regions of steep orography, such as Greenland, where classical theories of fronts and cyclone arguably break down, some problems remain
- A 60 Mbyte cyclone database now exists, covering just under a year of 00Z global model forecasts (T+0, 24,..144) for an enlarged North Atlantic domain. For each cyclonic centre 111 diagnostic values are stored. Conveniently, and ‘fortuitously’, the period covered (2000) was exceptionally cyclonic in the UK sector. As an additional reference point an image which shows the surface pressure pattern, objective fronts and database cyclonic centres has been archived for each time frame in the database (example in Figure 1).
- Early analysis of the data has shown, for the first time, a ‘1-year climatology’ of warm front wave, cold front wave and barotropic low positions.
- Similarly, initial comparisons of forecasts and model analyses of frontal waves and barotropic lows suggests that there are no clear systematic errors in under- or over-deepening at the extreme end of the cyclone spectrum. However more modest features seem to be under-represented in forecasts compared to analyses.

6. Further Work

As this is a relatively new field, the scope for further investigation is considerable. Some ideas are presented below.

6.1 Analysis

(i) Further analyse the current database, with a view to:

- pinpointing model biases as a function of location, regime, temperature, jet strength, ...etc, and use other database diagnostics to help suggest possible causes.
- Devise a probabilistic forecasting tool which relates model jet strength (variables 98 and 104 in table 3) and/or other variables to the likelihood of low-level wind maxima exceeding specified thresholds. This would be complementary to the ensemble approach.

(ii) Evaluate whether tracking algorithms can be successfully applied to the cyclone data

- This may require data at higher temporal resolution.
- Inclusion of position error variables such as 16 in Table 3, for all cyclone types, may be very useful for providing a tolerance input to the tracking.
- If successful we will be able to construct and compare forecast and actual cyclone life-cycles, and construct statistics describing cyclone positioning and development errors as pdf's for different lead times, again providing guidance that complements the ensemble approach. Results may also suggest the lead time at which a deterministic forecast ceases to have intrinsic value.

(iii) Assess whether separation in multi-parameter space might be a reliable quantity for correct cross-validation of cyclonic features in different forecasts and analyses for the same validating time. One would aim to use database parameters that are reasonably well-conserved, such as theta-w and PV2 height, in addition, of course, to position. The uses of this would be similar to the uses of (ii).

(iv) Combine with imagery (radar/IR/WV) to form composites for different cyclone types, as a pattern recognition tool.

6.2 Development

- (i) Add missing diagnostics (table 3 and others) and re-generate database for 2000, but at 12-hourly intervals not 24.
- (ii) Expand to cover 'global' or 'extra-tropical' ($\geq 20N$, and $\leq 20S$) domains.
- (iii) Improve the temporal coverage of the data, to include 4 PGM runs per day at 3 or 6 hour intervals, and both GM runs at 12 hour intervals.
- (iv) Automate database updating by modifying program set to run in batch mode (requires PV-Wave problem to be solved).
- (v) Automate updating of a routine set of database statistics, as new forecast data arrives (pending successful completion of (iv)).
- (vi) Apply the database software to test or real-time data from the New Dynamics formulation of the UM. One would expect characteristics to differ from the current UM; indeed initial impressions are that the new formulation may currently be too energetic (Sean Milton, personal communication).
- (vii) Apply the database software to the mesoscale model (non-trivial!).
- (viii) Apply the database software to other operational models, or even ECMWF ensemble runs.
- (ix) Investigate commercial possibilities for selling the database (to e.g. insurance and risk prediction firms).
- (x) By inputting climate model runs, measure how the extreme end of the cyclone spectrum may evolve in different greenhouse gas scenarios.

Acknowledgements

Assistance provided by Keith Williams, Peter Panagi and Paul Davison during this project is gratefully acknowledged.

References

- Carroll, E.B., 1997. 'A technique for consistent alteration of NWP output fields'. *Meteorol. Appl.* **4**. 171-178.
- Deveson, A.C.L., Browning, K.A., Hewson, T.D. 2001?. 'A Classification of FASTEX cyclones using a height-attributable QG vertical motion diagnostic'. submitted to *Q. J. R. Meteorol. Soc* in Oct 2000.
- Deveson, A.C.L., 2000. 'The application of a height-attributable vertical motion diagnostic to the classification and evolution of extra-tropical cyclones'. PhD thesis, available from Dept. of Meteorology, University of Reading.
- Hewson, T.D. 1997. 'Objective identification of frontal wave cyclones' *Meteorol. Appl.* **4**. 311-315.
- Hewson, T.D. 1998a. 'Objective fronts'. *Meteorol. Appl.* **5**. 37-65.
- Hewson, T.D., 1998b. 'A Frontal Wave Database'. JCMM Internal Report No. 85. pp 20. Department of meteorology, Reading university.
- Hewson, T.D., 1999. 'Objective Identification of Fronts, Frontal Waves and Potential Waves'. A concluding report from the COST 78 project on Nowcasting. Proceedings of 4th European Conference on Applications of Meteorology, Norrkoping, Sweden, September 1999, pp.331-334.
- Hewson, T.D., 2001. 'The North Sea Storm of 30th October 2000'. *Weather*. To appear in March issue.
- Panagi, P. & Dicks, E. 1997. Met. Office Unified Model data, diagnostic graphics programs, and other observational data available from the JCMM through the aegis of the Universities Weather Research Network UWERN. JCMM internal report no 69. Department of meteorology, Reading university.
- Renfrew, I.A., Thorpe, A.J., and Bishop, C.H. 1997. The role of the environmental flow in the development of secondary frontal cyclones. *Q. J. R. Meteorol. Soc.* **123**. 1653-167